International Journal of Innovative Computing, Information and Control
Volume **8**, Number **10(A)**, October **2012**

ICIC International ©2012 ISSN 1349-4198
pp. 6515–6538

AN ACCURATE 3D LIVER SEGMENTATION METHOD FOR SELECTIVE INTERNAL RADIATION THERAPY USING A MODIFIED K-MEANS ALGORITHM AND PARALLEL COMPUTING

Mohammed Goryawala[1], Magno R. Guillen[2], Seza Gulec[3], Tushar Barot[3]
Rekha Suthar[3], Ruchir Bhatt[1], Anthony Mcgoron[1] and Malek Adjouadi[2]

[1]Department of Biomedical Engineering
[2]Department of Electrical and Computer Engineering
[3]Herbert Wertheim College of Medicine
Florida International University
10555 West Flagler Street, Miami, FL 33174, USA
{ mgory001; Magno.Guillen; sgulec; tbaro001; rsuth001; rbhat002; mcgorona; adjouadi }@fiu.edu

Received June 2011; revised November 2011

Abstract. *3-D liver segmentation is vital in computer-assisted surgery applications such as minimal invasive surgery, targeted drug delivery,tumor resection, and donor transplantation. This study describes development and evaluation of a novel liver segmentation paradigm in support of Selective Internal Radiation Therapy (SIRT). Since segmentation accuracy and computational simplicity are the two key features for evaluation, the proposed method couples a modified k-means based segmentation and localized-contouring algorithm to obtain segmentation with high accuracy, based on an optimal number of slices. Furthermore, parallel computing is used to reduce the high computational load required of the process. Minimal manual interaction was required in the form of initialization with no correction or adjustment done during or after the process completion. Five rounds of experiments were performed to determine the accuracy and computational performance of the segmentation algorithm. Results were assessed by comparing volumes obtained from the segmentation algorithm to those obtained by manual segmentation done by experts. Statistical analysis is also carried out to determine if the same accuracy is obtained during multiple runs of the dataset and to determine if the manual initialization has any impact on the accuracy of the results. An average accuracy of 98.27% was achieved in estimating the liver volumes with consistent results obtained in various runs and independently of the user initializing the task. A reduction of 78% in computational time was accomplished by the parallel computing techniques in support of the lengthy segmentation process. Since SIRT requires accurate calculation of the liver volume, this new method provides highly accurate and computationally efficient process required of such challenging clinical requirements.*

Keywords: Image segmentation, 3D reconstruction, High performance computing, Modified k-means algorithm, Contouring, Performance metrics

1. **Introduction.** The American Cancer Society estimates that nearly 18,000 people are diagnosed with liver cancer annually. This unfortunately makes 1 out of 183 individuals born today susceptible to liver cancer at some point during their lifespan [1]. Liver cancer treatment which delivers maximum radiation dose to the tumor and minimum toxicity to the surrounding healthy tissue has been one of the major challenges in clinical practice.

Selective Internal Radiation Therapy (SIRT) with Yttrium-90 (Y-90) microspheres is emerging as an effective liver-directed therapy [2]. The treatment involves the accurate

calculation of functional tumor volumes and anatomical volumes of liver for the determination of the tumor to normal liver ratio and consequently for the calculation of the dose of Y-90 microspheres [3].

Present techniques for the determination of the anatomic volume of the liver involve tedious manual segmentation of the liver from the Computerized Tomography (CT) scans. The number of slices in a CT dataset varies from 200-400, which makes the task of computing the volume of the liver manually excessively tedious and time consuming. Also, the task is greatly dependent on the skill and proficiency of the technician/doctor, which could contribute to human error and skew the results.

This study proposes the development and implementation of a semi-automatic algorithm for the segmentation of the liver and tumor from Computed Tomography (CT) scans and the calculation of the volume of the liver for SIRT treatment.

Image segmentation is an important preprocessing step in many image processing applications including complex task such as brain segmentation from MR images [4,5], lung segmentation from CT images [6,7], and other medical image analysis [8]. Current automatic and semi-automatic procedures for liver segmentation are based on techniques that rely on (1) shape constrained segmentation using heuristic approaches [9], local shape models [10], atlas based techniques [11,12] or nonlinear models [13,14]; (2) rule based segmentation [15]; (3) gradient vector flow [16-18]; and (4) two or three dimensional region growing [19,20]. Although these techniques offer highly accurate results the algorithms need to accommodate varying protocols, data from different sources, artifacts, and the presence of pathological structures such as tumors [21,22]. Also, segmentation algorithms used in cases of liver segmentation tend to be difficult to operate for a person with limited amount of know-how of the conditions and requirements necessitated by these different segmentation techniques.

We aim to develop an algorithm which accurately segments and determines the volume of the liver but at the same time is easy to operate from a physicians point of view. The algorithm requests for minimal intervention in the initialization process and provides the complete analysis of the segmentation results automatically. The main objective of the algorithm is to provide the means to perform the calculations of the volumes to a high degree of accuracy with a much reduced computational time.

The main contributions of this study include: (1) establishing a new hybrid approach which utilizes the k-means based segmentation algorithm coupled with a new application of a localized contouring algorithm specifically for CT datasets, based on local regional thresholds defined in a small region around the point of interest in terms of relative radio density; (2) developing a process for liver volume calculations on the basis of an automated process that selects an optimal number of slices that will yield the highest accuracy possible minimizing as consequence human intervention on only 4 to 5% of any given dataset in the initialization process, and (3) proposing a parallel approach that reduces considerably the computational requirements for segmentation as well as volume calculations.

In order to overcome inherently high computational requirements that tasks such as segmentation and volume calculation demand a parallel computing process within a single desktop computer is employed. Tasks such as liver segmentation process and volume calculations are hence distributed across the cores/processors of the computer. Parallel computing has been widely used for reduction of computational times for image segmentation tasks particularly medical image segmentation [23].

MatLab provides effective different alternatives to address computationally-intensive tasks based on issues of parallelism and high performance computing (HPC). Krishnamurthy et al. presented an exhaustive description of all the HPC techniques offered by

MatLab [24]. The most popular techniques are MatLab-MPI [25,26], MatLab [27], Star-P [28,29], the MatLab Distributed Computing Toolbox (DCT) [30] and the Parallel Computing Toolbox (PCT) [31,32]. In this study, PCT and DCT are selected to set up the parallel computing network. This computational process is structured in a way that its deployment can extend to clusters and grids [33], if the need arises.

The infrastructure used for our experiments required the configuration of a job manager and a client host machine. The job manager schedules and coordinates the execution of jobs and tasks evaluation. The client host machine can request to the job manager a specific job and its related tasks, in which case a MatLab session (client session) is initiated. Moreover, a MatLab host machine through the MatLab DCT toolbox can be requested to execute a given task, in which case each MatLab session is called a worker, which behaves as a computing server. Since a given host machine can initiate several MatLab sessions, then it can hold several workers. The actual number of workers held by a given host machine depends on the resources available to it.

2. **Research Aim.** The research aim is to design a new algorithm for accurate and fast liver volume calculation using minimal user intervention while maintaining high accuracy in volume rendering. This algorithm semi-automatically segments the liver region from 3D CT scans. The algorithm extracts the liver region and renders the segmented liver for 3D viewing. The algorithm is also structured as a parallel-aware process so that a computationally-taxing task can be distributed over various computing nodes.

3. **Methodology.** Liver segmentation based on CT images is a challenging task due to the presence of similar intensity objects in the abdomen with no clear delineation between these objects and the liver. These objects include the spleen, stomach, wall of the abdomen, and kidneys. A new method for liver segmentation has thus been developed based on a combination of a modified k-means clustering process and the active contours algorithm. The implementation strategy is illustrated in Figure 1.

The novelty in this algorithm is in the manner the modified k-means based segmentation is used in combination with a localized contouring algorithm. This k-means segmentation approach requires the identification of five separate regions of the input CT images, which is one initial subsidiary contribution of this paper. A key contribution is the development of a new application of a localized contouring algorithm, based on local regional thresholds defined in a small region around the point of interest, which has not been developed for actual CT datasets. Pixels in an image obtained by CT scanning are displayed in terms of relative radio density rather than the traditional gray level intensity. The CT images are segmented keeping the pixel values in the Hounsfield units (HU). The HU value will be used to identify the liver tissues in the CT images. Typically the liver window is defined between -40 HU and 180 HU.

Although reduced manual interaction is desired, the variations in the liver datasets seen in patients having tumor along with the need to obtain accurate volume determination for the SIRT treatment justify the use of the proposed semi-automatic method. The proposed method used to select the slices requiring human interaction is based on tracking the changes observed in the liver region across the slices.

Moreover, the integration of parallel computing to solve liver segmentation has been reported in the literature; however, the incorporation of MatLab based parallel computing for liver segmentation purposes has not been explored as a more user-friendly and common platform. The ease and advantages MatLab based parallel computing offers over complex parallel computing systems is noteworthy.

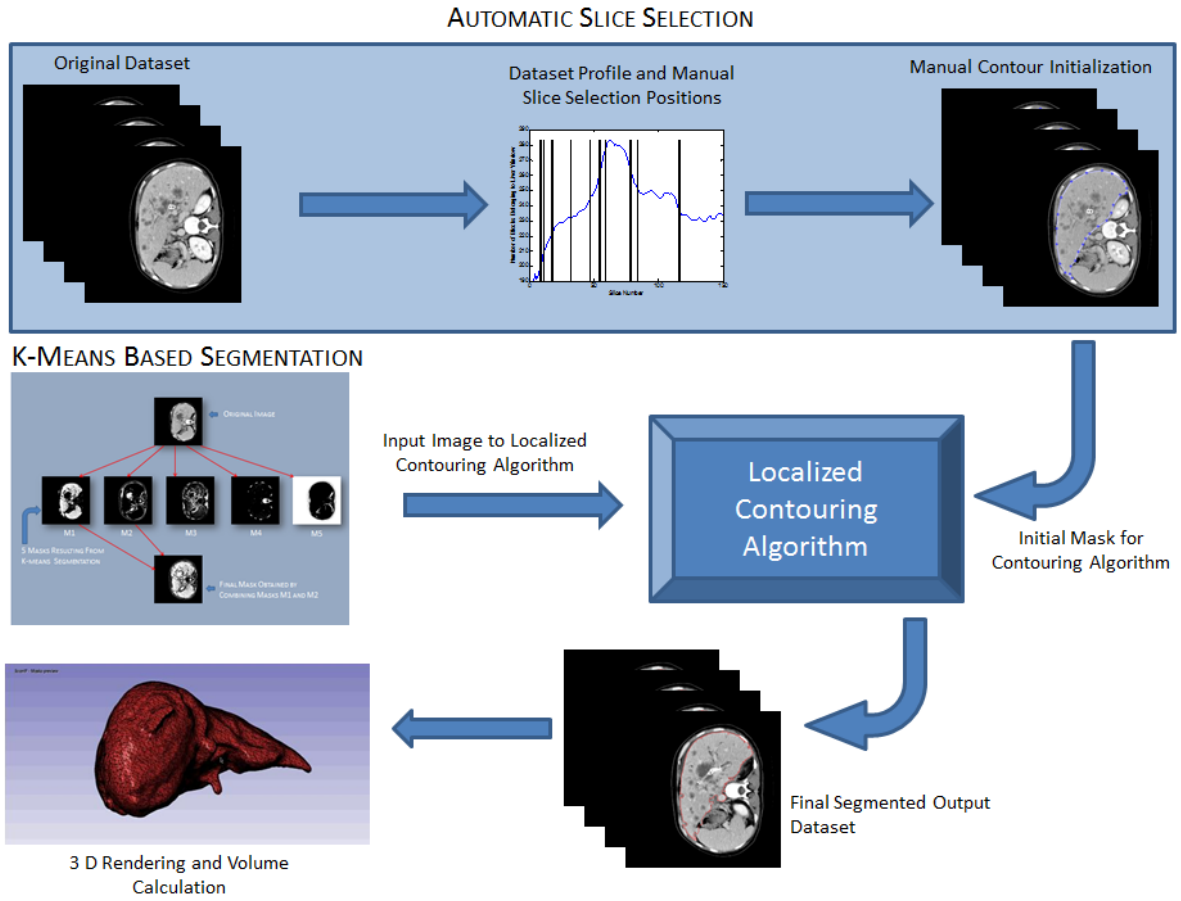

FIGURE 1. General algorithm for 3D liver segmentation and rendering

The CT scans of the patients are de-identified on-site. This process of de-identification is performed to conform to the Internal Review Board on human subjects (IRB approval 051810-01) and to the standards and guidelines established by the Department of Health and Human Services-HIPAA.

3.1. **Design structure of the algorithm.** At this juncture, the algorithm as designed requires the user to manually pick 5 points of varied intensity in the scan for the k-means segmentation as well as a rough outline of the liver in up to 5 widely spaced slices throughout the given CT dataset. From this initialization process, the following automated steps are then considered.

3.1.1. *The modified k-means algorithm and its suitability to liver segmentation.* This is a traditional clustering technique which tries to partition the given dataset points into various clusters whose means are similar [34,35]. The k-means algorithm as used here aims to minimize the squared Euclidean distance for clustering the data points to their respective groups. In the case of the images to be segmented, the data points are pixels which are to be clustered around the mean intensity or the pixels apriori chosen by the user.

The points are clustered based on the intensity of the selected points by minimizing the objective function U as defined in Equation (1).

$$U = \sum_{i=1}^{k} \sum_{x_j \in S_i} (x_j - \eta_i)^2 \tag{1}$$

where k represents the number of clusters S_i, with $i = 1, 2, \ldots, k$; and η_i is the intensity of the selected point, while x_j represents each point that belongs to cluster S_i ($x_j \in S_i$). In the case of liver segmentation, the CT slices are portioned into five regions whose mean intensity levels can be given either by the user or preset. The five regions manually identified on each CT slice are:

1. Liver
2. Surrounding organs
3. Peripheral Muscles
4. Ribs/Spinal cord
5. Outside of the body

The segmentation algorithm using the k-means yields 5 masks namely M1 through M5 corresponding to the aforementioned 5 regions as depicted in Figure 2.

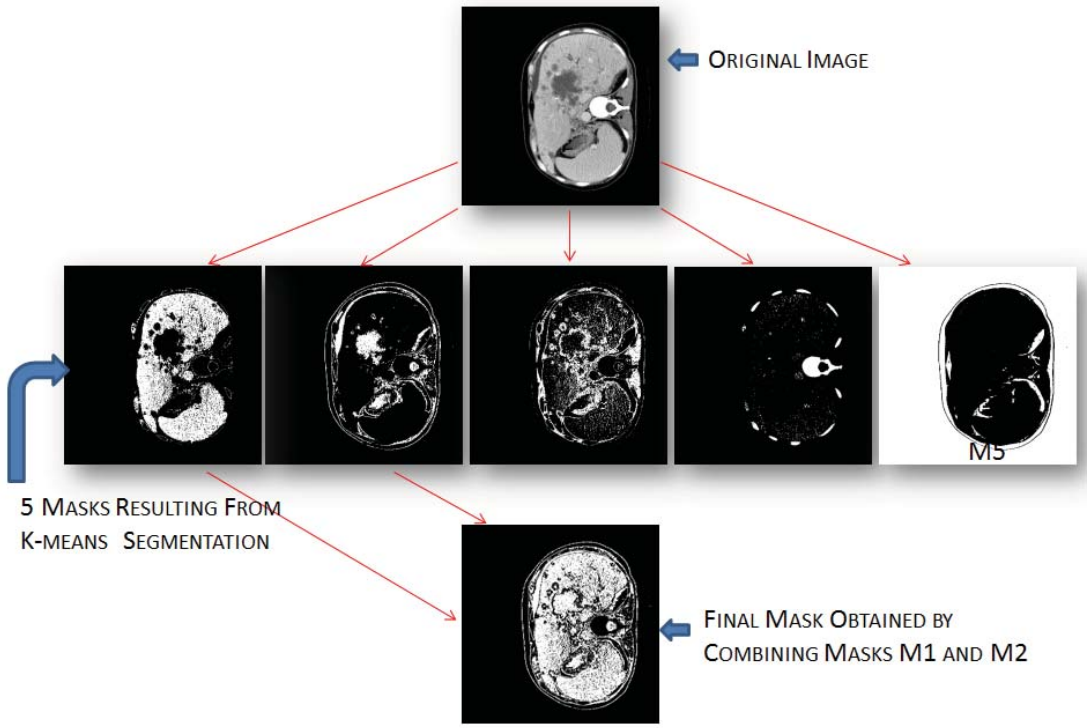

FIGURE 2. The 5 reference regions, M1 through M5, needed to apply the k-means based segmentation method on a liver CT dataset

Selection of the seed points for the k-means algorithm is an important feature for the algorithm. A random selection of seeds for the clusters as shown in Figure 3 results in the generation of incorrect masks. This is due to the clusters being formed around those random seeds which range from –1024 HU to 3000 HU for a typical CT slice. Since the liver was typically seen in the –40 HU to 180HU range random selection of seeds provides very less probability to achieve the required feat.

In case of uniformly selected points in the range of the CT acting as seeds, the centroids are centered around –1024 HU, –205HU, 614HU, 1433HU and 2252HU. These seeds fail to segment the regions containing the liver from the image as seen in Figure 3. An alternative would be to use uniformly selected seed points in the –40 HU to 180 HU liver range. Empirically, however, such a selection of seeds yields centroids too close to one another for suitable segmentation. Also a large number of points below –40HU and above 180 HU were misclassified and marred the resultant masks.

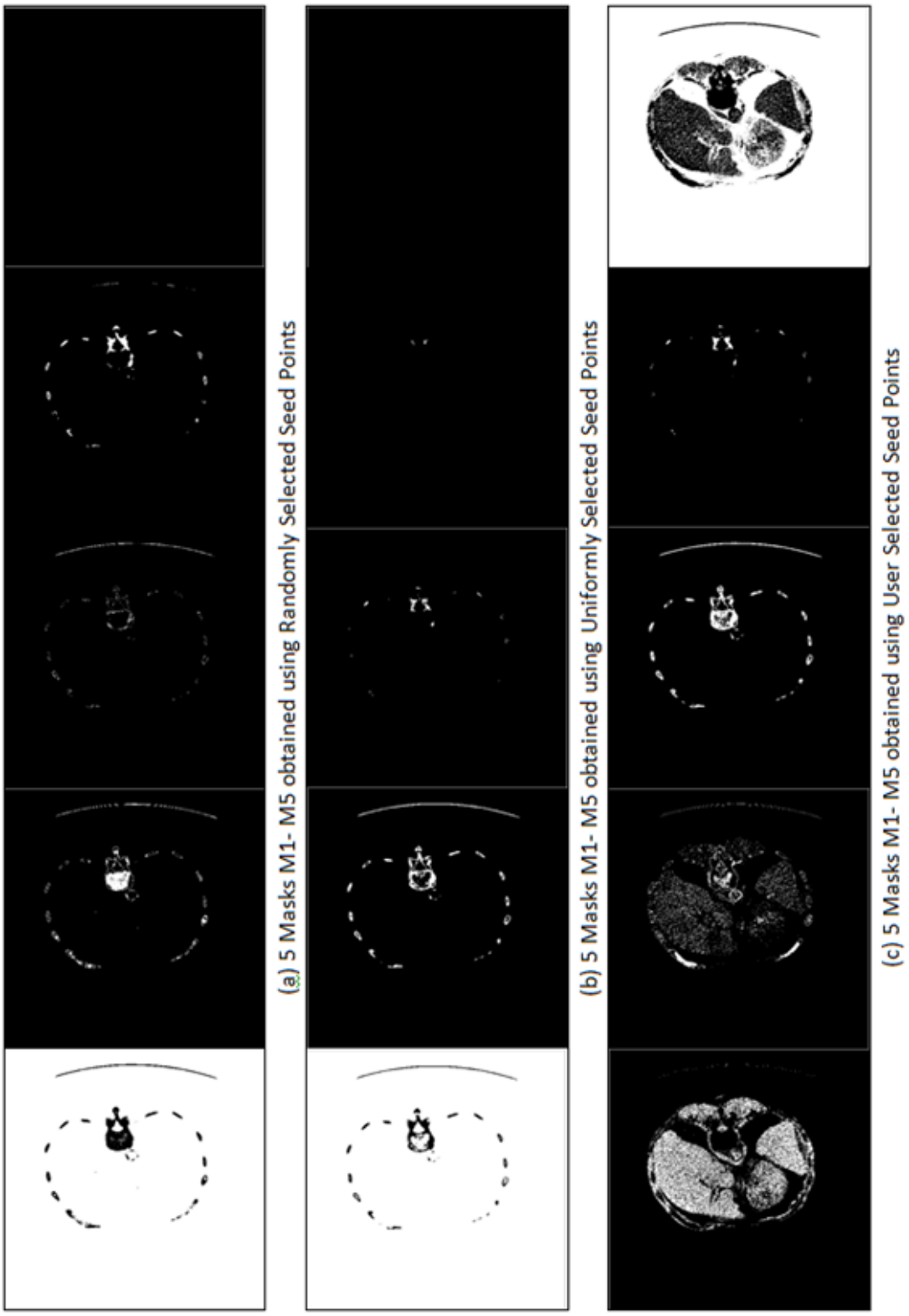

FIGURE 3. Selection of seed-points for k-means based image segmentation step

Hence, the modified k-means approach as deployed in this study segments effectively the different regions of the CT slice around the user selected points. The user selected points act as the seeds for each of the aforementioned five masks. The selection of the seeds, rather than a random selection or uniform selection of points in the entire intensity

range of the image, yielded much better segmentation results as shown in Figure 3 for any given slice. These seed points clearly differentiate the various organs of interest as compared to the other two methods of seed selection where the liver region is not at all visible.

Also segmentation of each image is replicated 3 times to achieve better results. The intersection of the results of the 3 segmentation runs for each image slice is taken to obtain the final segmentation. Selection of the intersection of the 3 runs provided results which were free from misclassification experienced using a single run. Lastly, the modified k-means is operated on a so called online update mode where the sum of distances is calculated with the movement of every pixel to a different cluster. Although this step is slightly more time consuming than when using a batch update, higher accuracies are however guaranteed since the local minima of the distance function can be calculated more accurately.

Another important finding of this study is in determining that the first two masks namely liver (M_1) and surrounding organs (M_2) can be utilized to effectively segmented the image. The masks M_1 and M_2 are in this case ORed together to obtain the final mask (M_{final}) as calculated in Equation (2).

$$M_{final} = M_1 + M_2 \tag{2}$$

This final mask is what is applied on the CT slice for segmenting the liver region. Based on empirical results, it was determined that the optimal mask would require a combination of the first two identified regions since in some cases the entire liver is not seen in mask M_1 due to the inhomogeneous intensity distribution across the entire liver region in the CT scans. The selection of masks M_1 and M_2 in combination ensures that no part of the liver is missed out.

In order to demonstrate the merits of the modified k-means approach, Figure 4 shows the results of applying the modified k-means as compared to the traditional k-means approach for segmenting the liver. Part (A) of Figure 4 demonstrates the differences obtained in the masks M_1 and M_2 and the mask M_{final} for the input CT slice shown. Figure 4 (a2-a4) show the result obtained using the modified k-means and Figure 4 (a5-a7) show the results obtained using the traditional k-means approach. It is observed that M_{final} obtained using the traditional k-means over estimates the liver region.

An observation from Figure 4(A) would indicate that only using mask M_1 from the traditional k-means approach would yield the required liver region. In order to show that this is not actually the case for every slice, results for another slice of the dataset is shown in Part (B) of Figure 4. Figure 4(B) demonstrates the need of using the mask M_{final} as obtained in Equation (2). Note that by using only mask M_1 for either the modified or the traditional k-means would results in the underestimation of the liver region.

The segmented image (S_1) after the modified k-means clustering is obtained by applying Equation (3) as follows:

$$S_1 = M_{final}.I \tag{3}$$

where S_1 is the image after the k-means clustering and I represents the CT image slice being analyzed.

3.1.2. *Initialization of the contouring-based segmentation.* The next step of the algorithm is the contouring based segmentation process. One of the major issues that concern contour based segmentation processes is the initialization of the contour. This contour based segmentation algorithm takes a user defined mask as input for the initialization algorithm. The user marks the approximate boundaries of the liver using a mouse pointer in slices which are widely apart from one another. Moreover, the selection of the slices in

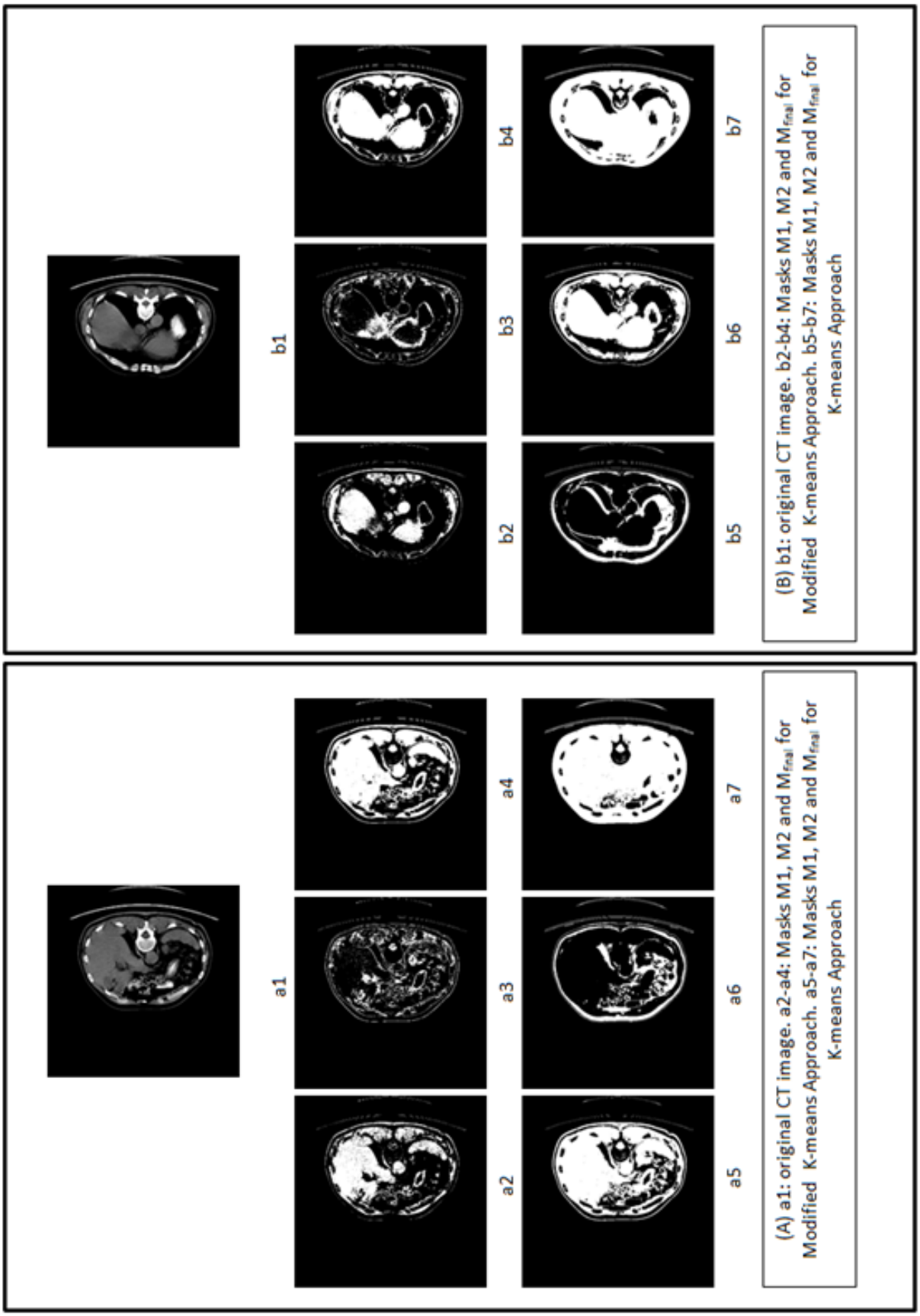

FIGURE 4. Comparison of the modified k-means method and traditional k-means method

which the user picks the initial contour depends on the change in information (presence of liver) from slice to slice. This is obtained by first dividing the entire image S_1 into blocks of 16×16 pixels. The selection of blocks of 16×16 pixels was determined to be the best solution.

Inside each block, the pixels that fall in the abdominal CT window of –40HU to 180HU were counted. A block was marked as being part of the liver region if at least more than half of the pixels were found in the abdominal CT window as described in Equation (4). Thus,

$$block\ \ marked = \begin{cases} 1 \text{ if } n/N \geq 0.5 \\ 0 \text{ otherwise} \end{cases} \tag{4}$$

where n and N are the number of pixels in the abdominal window and the total number of pixel elements in the block, respectively. Recall that $N = 16 \times 16$ was the window size selected for segmentation of the liver datasets presented in the results section.

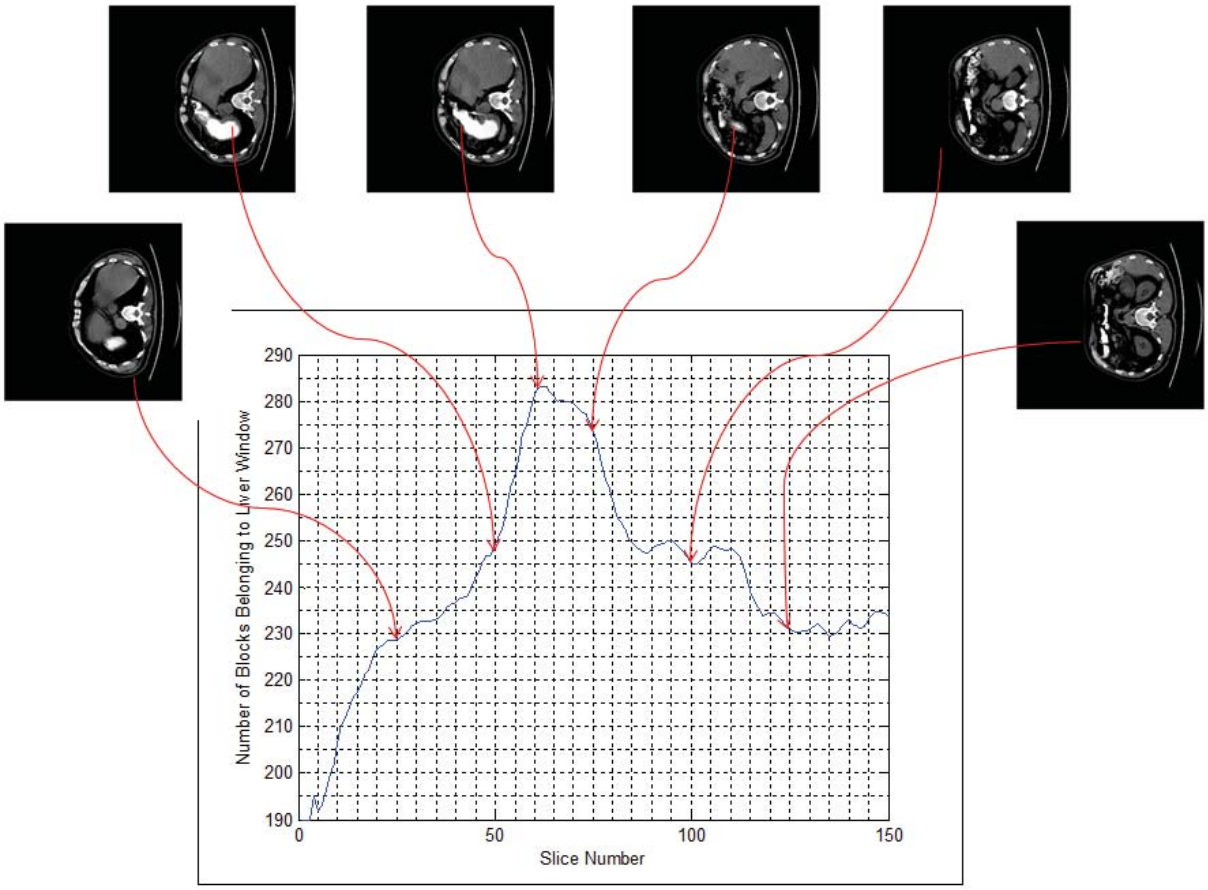

FIGURE 5. Generation of dataset profile curve depicting the slices corresponding to the marked points on the dataset profile curve

Figure 5 shows a typical profile curve for dataset 1 which displays the number of blocks belonging to the liver window as a function of the slice number in a particular dataset and the slices used to calculate the value of the curve at some particular instant of time. Such a curve gives the estimate of the changes in the size as well as the potential extent of the liver region seen across slices, providing as a consequence the information needed to select those slices which most probably contain a large portion of the liver region.

The first slice of the CT dataset was always selected for manual contour initialization. In this algorithm, in order to minimize the number of slices considered for contour initialization, a subsequent slice would need to show a 5% change in the number of blocks marked as in Equation (4) with respect to its predecessor. The intermediate slices which are not selected for manual initialization used the same initial contour as the slice closest to it in the dataset. This approach yielded around 4-5% of the entire dataset to be initialized by the user, rather than the time consuming slice by slice contouring of the entire dataset that is seen in clinical practice. The process yielded segmentation results that were not affected and the volume measurements that were highly accurate.

As an example, the slices chosen for manual initialization are marked by the black bars in Figure 5 for a particular dataset.

3.1.3. *Localized-region-based active contouring algorithm.* Once the initialization for all the slices of the dataset is obtained interactively, a localized-region-based active contouring algorithm is employed. Localized region growing algorithms are more robust than contouring algorithms not based on global energies for segmenting heterogeneous objects like the liver [36].

Let C denote the closed contour, such that $C = x|(x) = 0$ is a set of zero level for the signed distance function. The interior and the exterior of the contour are defined using the smoothened approximation of the Heaviside function. The interior of the closed contour C is defined in Equation (5) as

$$H\phi(x) = \begin{cases} 1, & \phi(x) > \epsilon \\ 0, & \phi(x) < -\epsilon \\ \frac{1}{2}\{1 + \frac{\phi}{\epsilon} + \frac{1}{\pi}\sin\frac{\pi\phi(x)}{\epsilon}\}, & \text{otherwise} \end{cases} \tag{5}$$

In reference to Equation (5), the exterior of closed contour C can then be expressed as $\{1 - H\phi(x)\}$.

In order to calculate only the local energies, a masking parameter α is introduced in the algorithm. The parameter defines the radius of the circle around the contour which has to be masked in order to calculate the local energies. This localization radius is defined in terms of the size of the image and its value is calculated as shown in Equation (6).

$$\alpha = \frac{1}{4}(P_r + P_c) \tag{6}$$

where P_r is the number of rows in the image and P_c is the number of columns in the image. The mask generated by using the above value of is given by Equation (7).

$$M_\alpha = \begin{cases} 1 & ||x - y|| < \alpha \\ 0 & \text{otherwise} \end{cases} \tag{7}$$

The algorithm incorporates the well-known Chan-Vese energy paradigm to model the interior and the exterior of the contour for segmentation [37]. The localized version of the Chan-Vese energy function is given by Equation (8),

$$E_{CV} = \int H\phi(y)(S_1(y) - \mu_{int})^2 + (1 - H\phi(y))(S_1(y) - \mu_{ext})^2 dy \tag{8}$$

where μ_{int} and μ_{ext} are the mean intensities of the interior and exterior regions of the contour, respectively. The localized versions of the mean intensities are obtained by restricting the field of view only to the masked region given by masking the image with M_α.

3.2. **Need for parallel processing.** This approach has resulted in successful and highly accurate segmentation of the liver as will be detailed in the *results* section; however, as in most 3D applications that include large datasets, this required inordinately lengthy processing time. This drawback is due to the fact that the algorithm operates on a slice by slice basis on the complete CT dataset. Each dataset is comprised of 200 to 300 slices. Our intention is thus to lower the processing time of the liver segmentation process so we can offer a reasonable and affordable solution for doctors and hospitals in tasks that rely on 3D rendering.

TABLE 1. Liver dataset specifics

Data Set Identifier	Number of Slices	Resolution of Images
1	155	512×515
2	320	512×512
3	320	512×512
4	217	512×512
5	442	512×512

Parallel computing is employed to reduce the computational times by distributing the task between more than one core/processor available on a single workstation, where a number of slices of the dataset will be processed simultaneously.

Taking into consideration the performance of the parallel computing algorithm, the liver segmentation is performed on images of size 512×512 pixels on unenhanced CT images [38]. The number of slices for the 5 datasets ranged anywhere from 150 to 450 as shown in Table 1. All datasets were de-identified and provided by North Jackson Hospital, which has a renowned liver cancer program.

Each dataset is processed using the in-house developed algorithm for segmenting the liver from abdominal CT images. The steps of the segmentation process for both sequential and parallel approaches are provided in Figure 6 and Figure 7, respectively.

The algorithm/process developed here segments the liver up to eight slices at a time. Once a given worker has completed the segmentation in a particular slice it picks up another slice from another set in the pool and starts the process in the new slice.

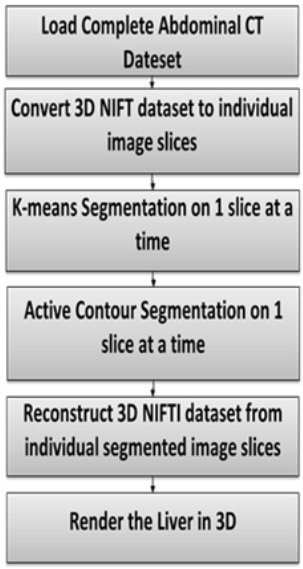

FIGURE 6. Flow diagram of serial approach of segmentation algorithm

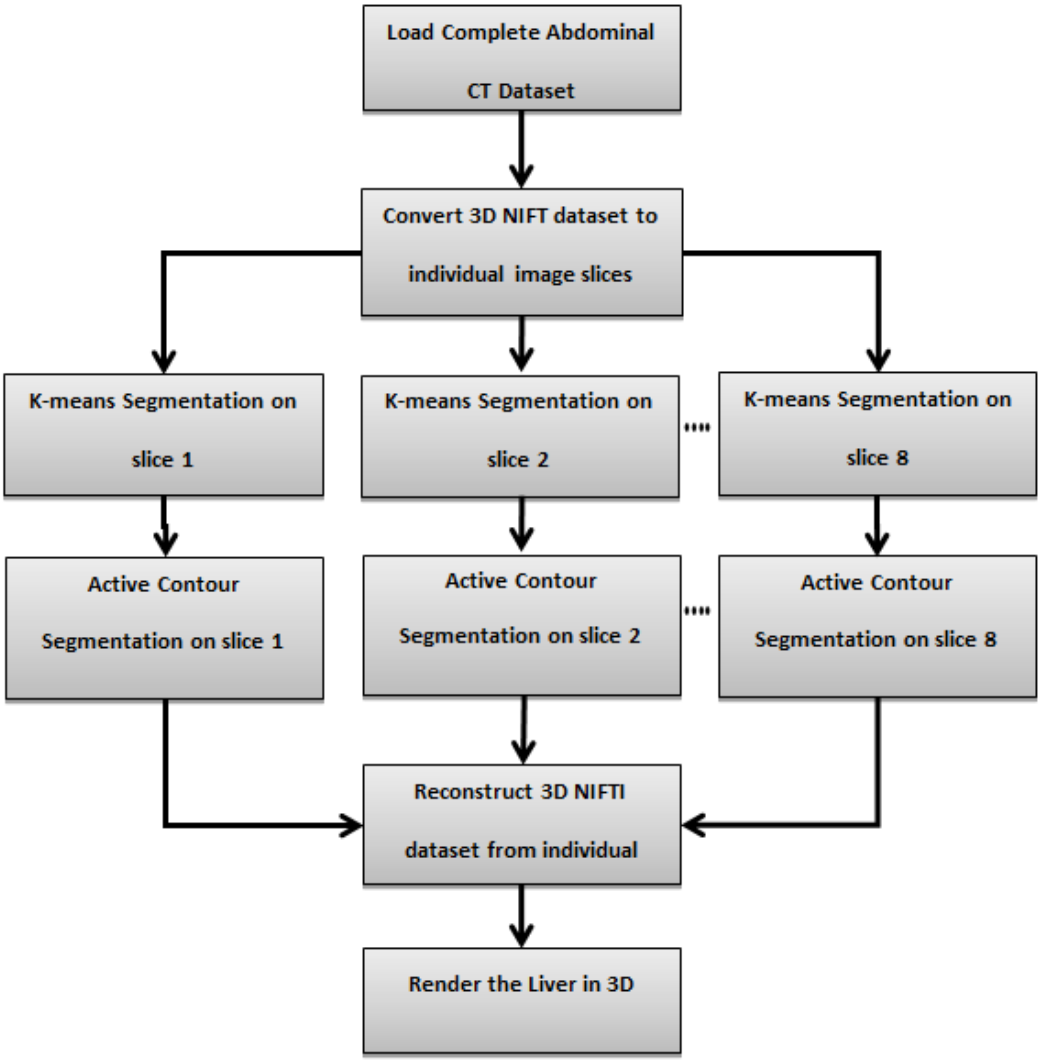

FIGURE 7. Flow diagram of parallel approach of segmentation algorithm

The steps followed for the setup of the parallel processing of the liver segmentation experiments were

– Define a job manager.
– Create a job and respective tasks as a request of the client host via MatLab script.
– Submit job to job queue for execution.
– Assess job results.
– Record timing.

The numbers of slices processed at a given time are dependent on the number of *workers* selected for the parallel processing task. In this experiment all the datasets are processed using 1, 2, 4 or 8 *workers* to estimate each time the computational gains achieved using parallel computing.

The expected improvement in the computational time T_c is referred here as the speed up of the process, and is computed using the following ratio:

$$T_c = \frac{C_1}{C_n} \tag{9}$$

where C_1 and C_n denote the computational time required to complete the task using a single *worker* and *nworkers*, respectively.

3.3. **Three-dimensional image rendering.** The 3D datasets are rendered using cost-effective third party software called ScanIP developed by Simpleware Ltd. based in the United Kingdom. The software renders the segmented dataset in 3D space and offers the possibility for the physician to view/edit/correct the rendered liver if necessary. The software also calculates the volume of the liver by determining the number of voxels that are marked as being within the liver region by the segmentation algorithm. The only inputs fed to the software are the segmented dataset and the original resolution of the CT datasets. The calculated volumes are in milliliters (ml).

4. **Results.** The first part of this section provides the results for the automatic slice selection algorithm. The second part provides a comparison of the volumes obtained by the proposed algorithm in contrast to the traditional manual segmentation as performed by the medical staff. The third section provides the results for the speed improvement for the liver segmentation process achieved using parallel computing.

4.1. **Automatic slice selection.** The automatic slice selection algorithm aims at determining the slices that are to be manually initialized for the contouring algorithm. This algorithm calculates the change in the extent and structure of the liver shown across the slices by counting the number of blocks belonging to the liver as expressed by the range of –40 HU to 180 HU. This generates a profile curve for a particular dataset like the one shown earlier in Figure 5.

Since the block size is a parameter which can define the accuracy of the algorithm, we carried out the experiment using different block sizes. To evaluate the performance of the algorithm we introduce a new parameter ψ as defined in Equation (10),

$$\psi = |p - \bar{p}| \tag{10}$$

where p represents the number of the slice manually selected, and $\bar{p}$ is the number of the slice picked by algorithm. Figure 8 shows the parameter ψ plotted as a function of the block size.

Since ψ represents the distance between the true largest slice obtained manually and the largest slice obtained by the algorithm, a smaller value of ψ would indicate a better performance. Results in Figure 8 show that the lowest values of ψ are consistently seen

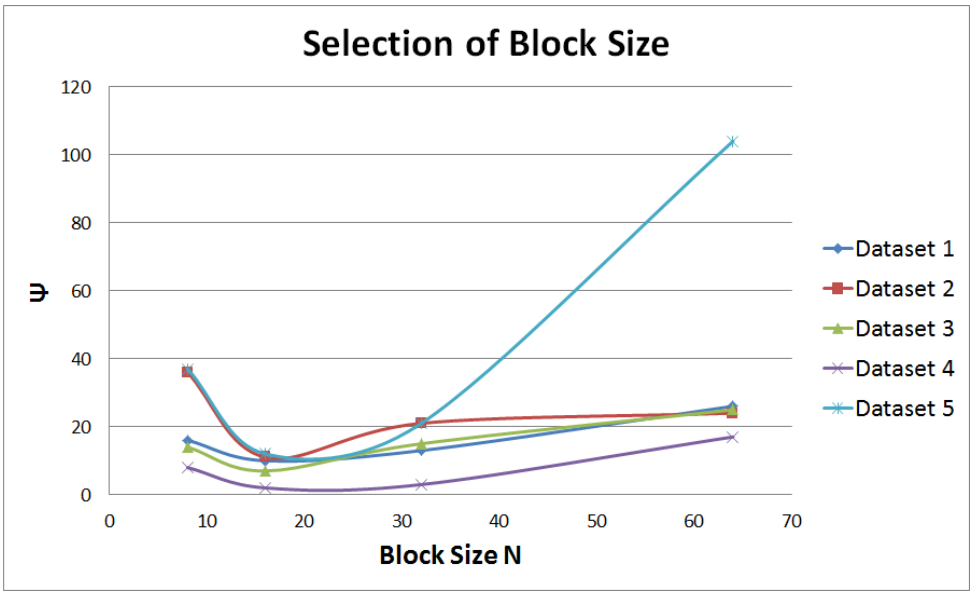

FIGURE 8. Selection of block size based on ψ performance

for block size 16×16. Also dataset 5 shows a very high value for block size of 64×64. This can be attributed to the presence of several smaller sized objects in the CT images such as duodenum whose intensity distribution is similar to that of the liver.

The computational time to obtain the profile curve was also monitored to obtain a relationship between the block size and the time required to generate the curve. Such a study is important to know if the profile curve generation is burdening the algorithms performance and if larger block sizes at the cost of accuracy is a likely option. Figure 9 shows the relative gains in computational time plotted as a function of the block size where the relative gain R is given by Equation (11).

$$R = \frac{\text{Computational Time required for Blocksize } 8 \times 8}{\text{Computational Time required for Blocksize } N \times N} \tag{11}$$

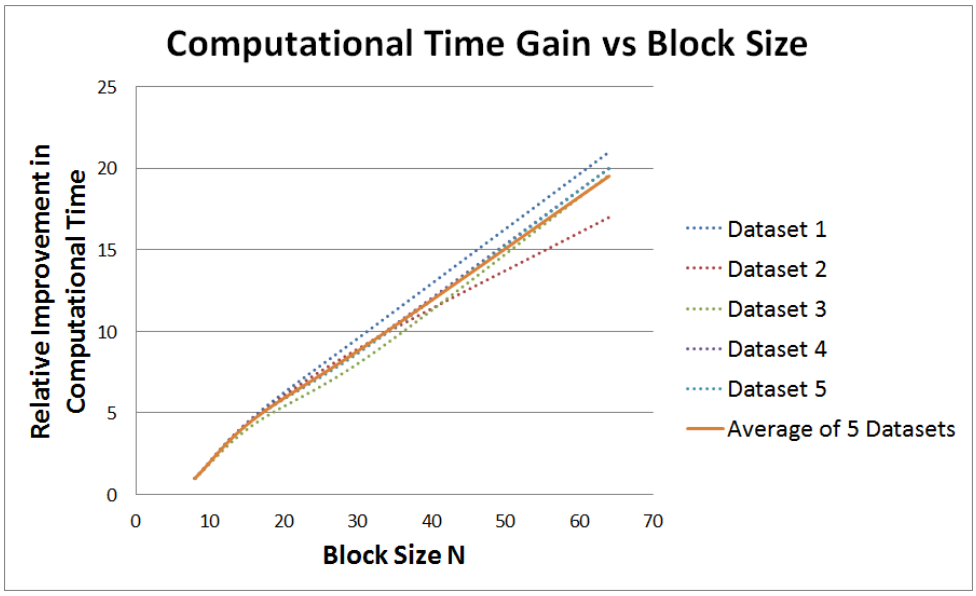

FIGURE 9. Computational time gain vs. block size results for the processing of 5 datasets

It can be seen from Figure 9 that the relative improvement in the computational time is linearly related to the block size. We see that the relative improvement in the speed by using a 16×16 block instead of 8×8 is around 3.6. It can be observed that as the block size is increased, the time to execute the automatic slice selection process reduces drastically with block sizes of 32×32 and 64×64, speeding up the process approximately 9 times and 19 times over an 8×8 block, respectively.

4.2. **Segmentation results.** The image data has been acquired using a combined PET/CT system (GE Discovery LS) with scanning parameters of 140 kVp, 80 mA, 0.5 s rotation time, and 512×512-pixel matrix. The images were provided in the DICOM format. Pixel sizes ranged from 0.54 to 0.97 mm. For each scan, a stack of 155442 slices covering the livers were acquired.

Figure 10 shows the segmentation results (shown in red) obtained for a particular dataset (Dataset 5). The figure shows 5 slices across the database. The slices are displayed in the [–40 180] window for the CT dataset.

Figure 11 displays the results for other datasets used in the validation of the algorithm. The point to be noted is that there is a great variation in the intensity, structure, position of the liver from dataset to dataset. Moreover, some of the datasets show the presence of tumors.

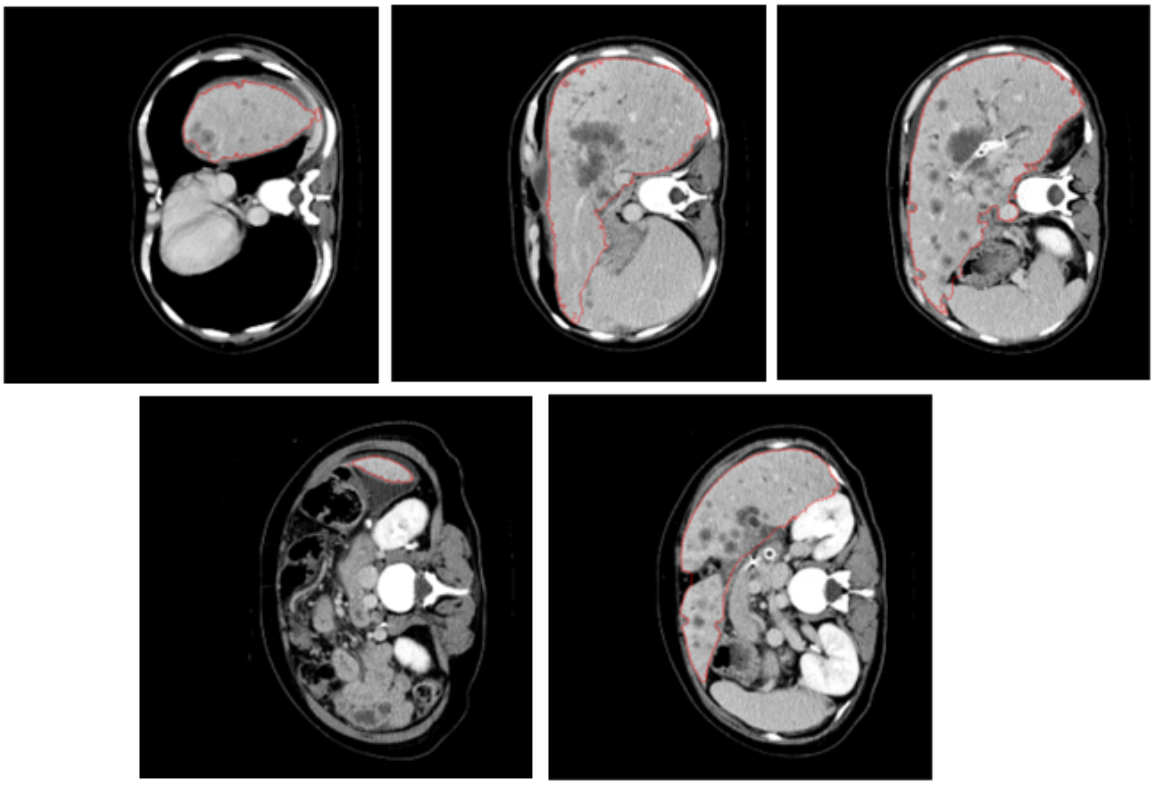

FIGURE 10. Five slices showing detailed segmentation results for dataset number 5

TABLE 2. Comparison of volumes calculated on 5 datasets

dataset	Volume Calculated by Algorithm (ml)			Average Volume of 3 Trials (ml)	Standarad Deviation of 3 Trials (ml)	Volume Obtained by Manual Segmentation (ml)	Absolute Difference between Calculated and Manual (ml)	% Error
	Trial 1	Trial 2	Trial 3					
1	1430	1429	1447	1435.33	10.12	1365.223	70.11	5.14
2	5370	5293	5353	5338.67	40.45	5336.282	2.38	0.04
3	3990	4056	4036	4027.33	33.84	4031.826	4.49	0.11
4	2580	2627	2596	2601.00	23.90	2656	55.00	2.07
5	2690	2640	2727	2685.67	43.66	2651	34.67	1.31
							Average	1.73

In order to validate the segmentation results obtained by the algorithm, the volumes of the extracted livers were compared to manually calculated volumes. The manual calculation was done by an expert and is treated as the gold standard for the comparison. Comparative results are shown in Table 2.

Table 3 shows a comparison between some of the current techniques and the proposed technique in terms of the accuracy and the computational times required to segment the liver. For the comparison of accuracy, the average volume difference between the calculated and the manual volumes is presented along with the standard deviation for

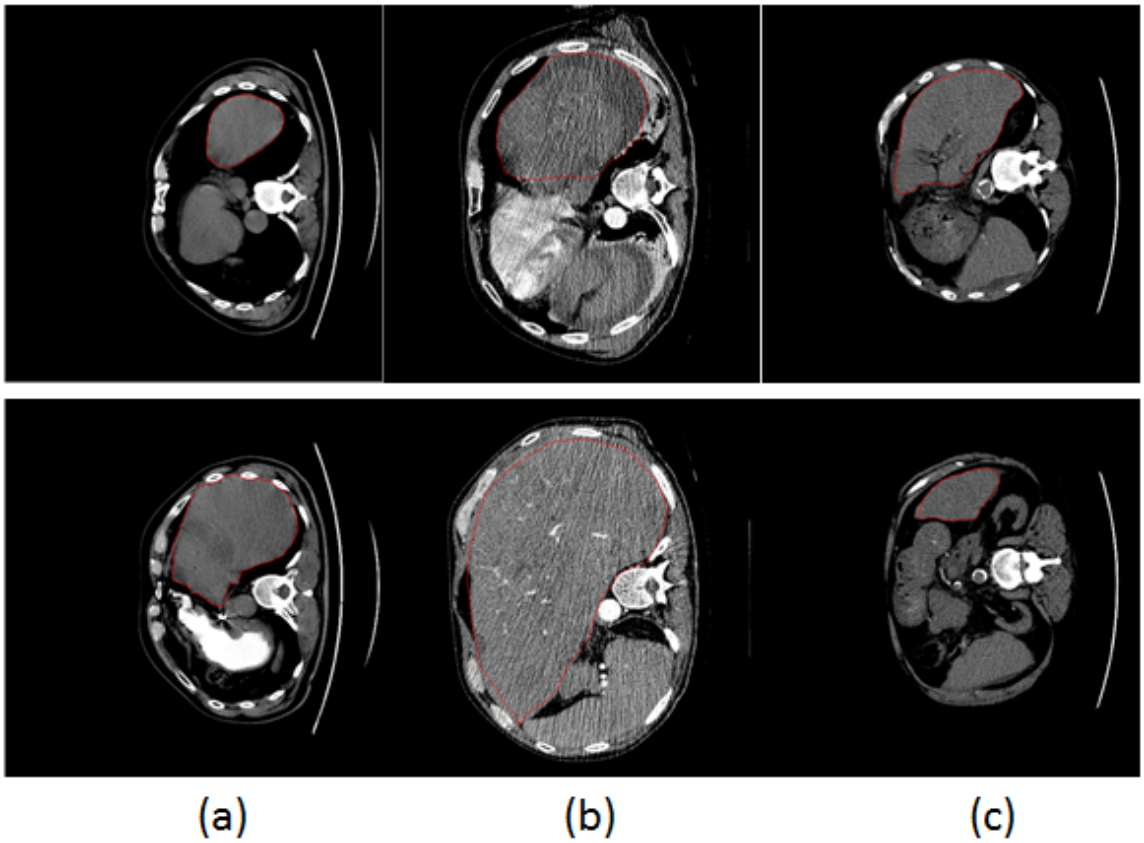

FIGURE 11. Example of segmentation results for other evaluated datasets. Each column shows two slices. (a) Dataset 1, (b) Dataset 2, and (c) Dataset 4.

the particular study. For comparing the computational times, Table 3 provides the time taken per slice to segment the entire dataset. Such a comparison is essential since different algorithms use datasets with different number of slices for the analysis which determines the time needed for processing the entire dataset.

Results of the 3D rendering process obtained from the ScanIP software are shown in Figure 12 for the different datasets (a) through (e). The 3D rendering displayed in Figure 12(a) is for the same dataset for which the slices were shown in Figure 10. The renderings shown here have solid surfaces and a mesh finish. However, translucent surfaces can be generated with varying opacities and colors if needed. The need to generate translucent surfaces would be useful to demonstrate the presence of a tumor inside the liver as an example.

4.3. **Statistical analysis on the segmentation results.** A statistical analysis is also carried out to determine if the changes seen in the calculation of the volumes between different trials is significant. Consequently, an Analysis of Variance (ANOVA) is carried out on the absolute error obtained during the various runs. Table 4 shows the errors in the various runs and Table 5 shows the results of the ANOVA.

The results of the ANOVA show that the trials are not a significant factor ($p > 0.05$), which establishes that the results of the proposed algorithm are indeed consistent.

In order to determine if the user initialization had impact on the results obtained by the algorithm, 3 users with different levels of knowledge in the field of medicine and engineering were asked to initialize the algorithm. The users were asked to rate themselves on their knowledge of liver anatomy and algorithms/programs on a scale of 1 to 5. Also,

TABLE 3. Comparison of volumes calculated on 5 datasets

Method	Volume Difference (% Error)	Processing Time per slice (sec)
Beck and Aurich [39]	1.82.5	3.00
Beichel et al. [40]	1.01.7	15.43
Chi et al. [16]	2.66.3	14.57
Dawant et al. [41]	2.52.3	8.57
Furukawa et al. [11]	–7.34.7	15.43
Heimann et al. [13]	1.73.2	3.00
Kainmuller et al. [9]	–2.92.9	6.43
Lee et al. [42]	1.32.9	3.00
Maasoptier et al. [18]	5.8%	11.40
Rusko et al. [20]	–3.86.4	0.21
Saddi et al. [14]	1.24.4	2.36
Schmidt et al. [15]	–4.93.0	8.57
Seghers et al. [10]	–6.82.3	12.86
Susomboon et al. [43]	–11.530	10.71
van Rikxoort et al. [12]	1.84.2	19.29
Proposed Algorithm	1.72.1	7.50

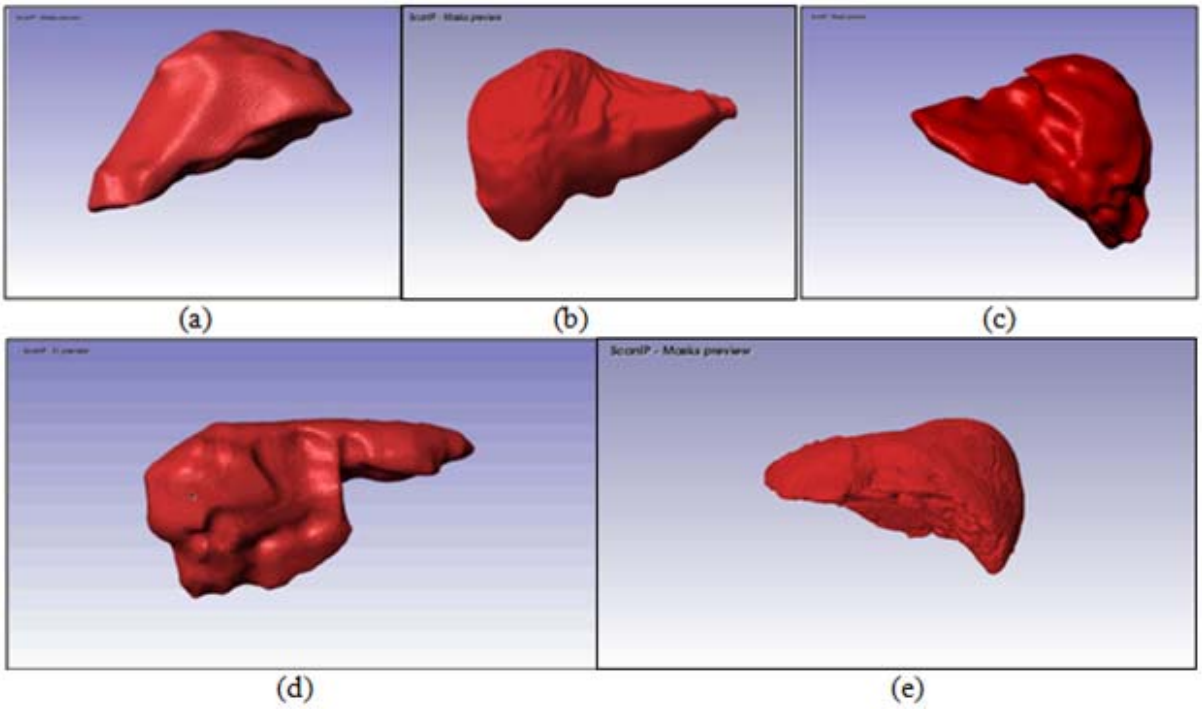

FIGURE 12. (a)-(e) Display 3D renderings of livers in dataset 1-5 using ScanIP software respectively

all users were given a basic understanding of the liver anatomy to help them identify the liver in the CT scans for the initialization purpose. Table 6 shows the profiles of the different users selected for the main purpose of testing the algorithm.

An ANOVA test was again carried out on the errors obtained after the segmentation process was initialized by the 3 users. The errors calculated as the absolute difference

TABLE 4. Absolute error obtained during the various runs

dataset	Absolute Error (Absolute of the difference between the calculated volumes by the algorithm and the manual volumes) (ml)		
	Trial 1	Trial 2	Trial 3
1	64.77	63.77	81.77
2	33.71	43.28	16.71
3	41.82	24.17	4.17
4	76	29	60
5	39	11	76

TABLE 5. ANOVA analysis of various runs

Source	Sum of Squares	df	Mean Square	F Value	p-value (Prob > F)	
Model	793.04	2	396.52	0.59	0.56	not significant
A-Trials	793.04	2	396.52	0.59	0.56	
Pure Error	7932.49	12	661.04			
Corrected Total	8725.54	14				

TABLE 6. Profile of users selected for the experiments

User	Knowledge of liver anatomy	Knowledge of Algorithms/Programs	Occupation
1	5	1	Medical Doctor/Oncologist
2	3	2	Biomedical Engineer
3	1	4	Electrical Engineer

TABLE 7. Absolute error obtained using different users for initialization

dataset	Absolute Error (Absolute of the difference between the calculated volumes by the algorithm and the manual volumes) (ml)		
	User 1	User 2	User 3
1	41.28	8.33	34.02
2	262.16	12.67	133.51
3	78.25	187.40	118.21
4	5.44	72.89	17.85
5	132.06	97.59	120.53

between the algorithm calculated volumes and the manual gold standard volumes are shown in Table 7 with the ANOVA results shown in Table 8.

In retrospect, these ANOVA results show that the error in the volume calculation is again not dependent on the user who initializes the dataset since the factor Users is not significant with a p-value of 0.84 ($p > 0.05$).

TABLE 8. ANOVA analysis of various users

Source	Sum of Squares	df	Mean Square	F Value	p-value (Prob > F)	
Model	2051.45	2	1025.73	0.17	0.8476	not significant
A-Users	2051.45	2	1025.73	0.17	0.8476	
Pure Error	73413.67	12	6117.81			
Corrected Total	75465.12	14				

4.4. **Parallel computing results.** This section presents the results of the liver segmentation process implemented on the Windows Vista platform. All experiments performed in this study were conducted on a system running Windows Vista based on an HP DC6700 computer equipped with two Intel Core 2 Quad Processor operating at 2.67 GHz with 8 GB RAM. The use of the software/hardware configuration was determined by benchmarking experiments using various hardware and operating system configuration[9].

Taking into account the performance of the parallel computing algorithm with different variables, the segmentation was performed on images of size 512×512. The number of slices for the 5 datasets ranged anywhere from 150 to 450 as indicated earlier in Table 1.

Figure 13 displays the computational time for the different datasets as a function of the number of workers employed for the task. We see that parallel processing reduces the time for the segmentation for dataset 5 from around 270 minutes to as low as 56 minutes. This is the highest processing time experienced among all the datasets since dataset 5 is the largest. The capability to complete the whole segmentation process in less than 1 hour as compared with 4.5 hours is a great improvement in context of hospitals efficiency. The results show a speed up of around 5 when 8 workers were employed, as seen in Figure 14.

5. **Discussion.** The results presented in Figure 8 show that a block size of 16×16 yields the best performance. For block sizes of 32×32 and 64×64, the number of pixels in a block is too large to make a correct estimate for the size of the liver. For block size

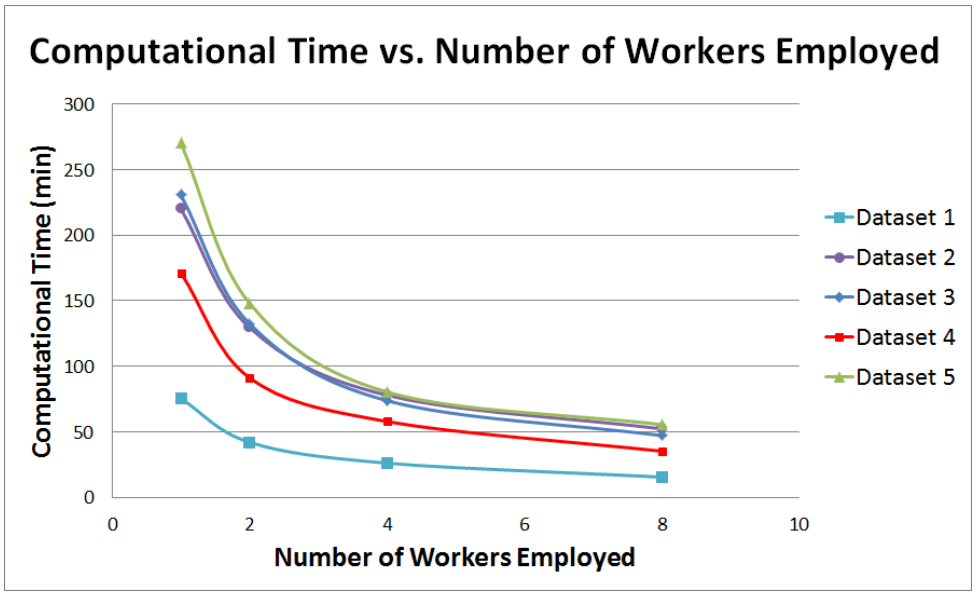

FIGURE 13. Computational times for liver segmentation

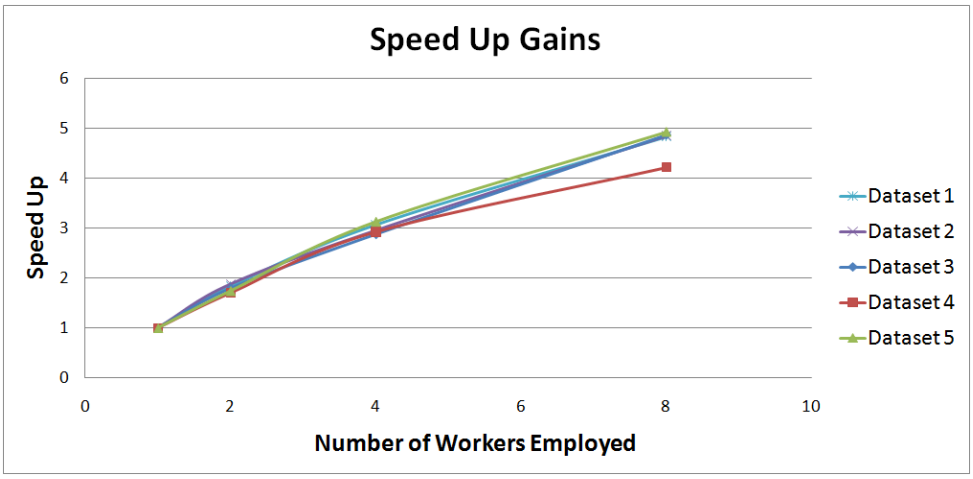

FIGURE 14. Speed up for liver segmentation

8×8 the amount of noise pixels in a block may be the reason for deviation from the best performance. Moreover, in the case of using 8×8 blocks, small regions of intensity similar to liver, but belonging either to the peripheral muscles or the duodenum, maybe selected as the liver region, as a consequence yielding incorrect results. Similarly small regions belonging to the liver might be missed in large block sizes.

Also, Figure 9 displayed that the computational time reduces as the size of the block is increased. This is intuitive since a larger block size results in fewer blocks to be analyzed. Moreover, the absolute time for calculation of the profile curve for any dataset using any block size is less than 2 minutes. Hence, the gains in computational time achieved are not substantial since the time for the contouring algorithm is too large. The use of the 16×16 block size is justified by the fact that the best accuracy is obtained for 16×16 blocks with an optimal processing time. Figure 4 displays a typical profile curve for a liver dataset with the black bars marking the position of the slices in which human interaction is needed. It can be observed from the figure that the number of slices picked for human initialization is directly related to how fast the liver volume is changing across the dataset. Hence, regions on the profile curve that have a higher slope or greater changes in the liver structure have more slices selected for human initialization. Regions which show little or no changes in the structure use the same initialization and hence a reduction in the human interaction can be achieved without compensating on the accuracy.

Figure 10 displays visually that the segmentation process is capable in extracting the liver region faithfully. The liver region is faithfully separated from the heart, spleen and other organs. Very little leakage to the adjoining organs is seen due to the use of local properties for the contouring algorithm. Also, Figure 11 displays that the segmentation is independent of the structure, size, position and intensity distribution of the liver region. It can be observed that the intensity distribution is not similar across the 3 liver datasets displayed in Figures 11(a)-11(c) and the algorithm faithfully identifies and segments the liver region. Also, the size of the liver is vastly different in Figure 11(a), where the patient has undergone an earlier resection. This makes the algorithm capable of use in post-treatment follow-up also.

Results displayed in Table 2 show that the volumes of the liver calculated by the algorithm are in agreement with that of the medical experts. Across the five evaluated datasets we see a mean accuracy of as high as 98.27%. Such a high accuracy is very advantageous for treatment planning in SIRT. SIRT relies on the calculation of the tumor to liver volume ratio for the calculation of the radioactive dose to the patient. Accurate

volume calculation specific to each patients anatomy would help in the calculation of the absolute precise dose to deliver to that patient. This would reduce the risk for excess dosing which may damage healthy surrounding liver tissue or on the other end of the estimation reduce the risk for under dosing and the potential relapsing of the tumor.

As seen in Table 3, the proposed technique is highly accurate in estimating the liver volume. An important feature to note is the low standard deviation in the volume calculation which suggests high consistency in the results. The algorithm fairs well in respect with the computational times required to segment the liver. It should be noted that since the algorithm is parallel aware and capable of being deployed on larger clusters, the computational times can be brought down considerably.

The results in Figure 13 show that the computational time for the segmentation process is reduced when parallel processing is incorporated in the process. The parallel processing is employed using either 2, 4 or 8 workers and the choice of the number of usable workers is dependent on the available hardware resources. The maximum number of workers that can be employed are dependent on the hardware resources. An increase in the number of workers in the absence of needed resources leads to system saturation with insignificant improvement offered by parallel processing. However, in a situation where hardware resources are plentiful great gains can be achieved. The results displayed in Figure 13 show the reduction in computational time for liver segmentation from approximately 250 minutes to as low as 50 minutes.

Figure 14 displays the gains obtained using parallel computing in terms of the speed up factor as defined in Equation (9). It is observed that an average speed up of 5 is obtained by incorporating up to 8 workers. The graph shows a fairly linear rise in the speed up with the number of workers and saturation for higher number of workers is not experienced for up to 8 workers. This is an important feature to be noted since it gives us the opportunity to further increase the number of workers in the future.

The distribution of the slices of the dataset are set such that one slice is processed by a worker at a time provides the opportunity of speeding the entire process up to $8\times$ theoretically for the system under use, but as a general rule, the maximum theoretical limit is given by the number of processors/cores that are present on the computer, and not by the number of workers. However, empirically, the hardware systems resource limits the speed up to approximately fivefold. Better computers with more resources such as processing power and memory, or distribution of the task over a cluster of computers which raises the number of configurable workers can provide higher speed up but with an added cost.

However, we have to be cautious in this reasoning since the parallelization of tasks is not possible on all algorithms, so there is an individual level of parallelism that applies to each algorithm. This reasoning suggests that the same gains may or may not be observed when parallelization is applied to any other liver segmentation algorithm. Also, as a note of caution, the reader should be aware that when installing the PCT/DCT in MatLab version R2008, a maximum of 4 local workers can be defined. However, the MatLab version R2009 allows defining a maximum of 8 local workers. This feature is independent of the hardware used, although the number of usable workers depends on the available system resources.

This study also highlights the advantage of developing algorithms aware of parallel computing in medical imaging, before investing in a large scale distributed system or an expensive parallel machine, providing opportunity for accelerating the image processing tasks and maintaining the accuracy of the procedure in a cost-effective fashion and by using a single desktop computer, especially in the advent of future processors with six or more cores on a single chip. This feature allows the algorithm to be easily portable

and adaptable in hospital settings with minimal space requirements. More importantly, beyond the computational gains that are made under the proposed approach, the hybrid algorithm introduced in this study displays a high accuracy in calculating the volumes of different livers with a minimal number of slices to be initialized by the user. Continuing future work aims at reducing the number of slices initialized by the user.

6. **Conclusions.** The paper demonstrated the development of a robust and accurate method for the segmentation of the liver from CT images for the purpose of volume calculations. The algorithm is independent of the dataset-properties namely structure, size, position and intensity distribution of the liver region due mainly to the novel hybrid segmentation method that coupled the k-means algorithm with a newly established contouring method that relied on radio density of the CT images. The experiment results reported in this study display very high accuracies of 98.27% in agreement with manual expert analysis.

Also, the development of the novel initialization method, which aims at reducing human/user interaction, achieved highly accurate results with only 4 to 5% of the dataset initialized by the user, minimizing greatly human intervention as a consequence.

The proposed algorithm is also structured to lend itself to parallel computing, which is viewed as an important characteristic in applications that require heavy computational loads such as in medical imaging. Parallel computing provided henceforth a scalable approach applicable for single workstations poised to serve as a portable method that is cost-effective and highly desirable in clinical settings.

The results obtained on the execution of the parallelization of the liver image segmentation indicates a significant speed up in the performance, achieving more than 500% increase by using 8 MatLab workers on a dual quad-core machine.

Also, SIRT relies on the calculation of the tumor to liver volume ratio for the calculation of the radioactive dose to the patient. Accurate volume calculation specific to each patients anatomy would help in the calculation of the absolute precise dose to deliver to that patient. This would reduce the risk for excess dosing which may damage healthy surrounding liver tissue or reduce the risk of under dosing and the potential relapsing of the tumor.

Acknowledgment. The authors appreciate the support provided by the National Science Foundation under grants CNS-0959985, CNS-1042341 and HRD-0833093. We also acknowledge the support provided by the University Graduate School through the Dissertation Year Fellowship for Mr. Mohammed Goryawala. The authors give special thanks to the Department of Oncology of the North Jackson Miami Hospital for their valuable clinical support and to the Ware Foundation for the generous philanthropic support they continue to provide.

REFERENCES

[1] A. Jemal, F. Bray, M. M. Center et al., Global cancer statistics, *Ca-a Cancer Journal for Clinicians*, vol.61, no.2, pp.69-90, 2011.

[2] W. Y. Lau, S. Ho, T. W. Leung et al., Selective internal radiation therapy for nonresectable hepatocellular carcinoma with intraarterial infusion of 90yttrium microspheres, *Int. J. Radiat. Oncol. Biol. Phys.*, vol.40, no.3, pp.583-592, 1998.

[3] R. Murthy, R. Nunez, J. Szklaruk et al., Yttrium-90 microsphere therapy for hepatic malignancy: Devices, indications, technical considerations, and potential complications, *Radiographics*, vol.25, pp.S41-55, 2005.

[4] N. Che, X. Che, Z. Gao and Z. Wang, The segmentation algorithm based on regional dynamic search for MR brain image, *ICIC Express Letters*, vol.5, no.8(B), pp.2957-2963, 2011.

[5] S.-G. Shu, H.-H. Lin, S.-W. Kuo and S.-S. Yu, Excluding background initial segmentation for radiographic image segmentation, *International Journal of Innovative Computing, Information and Control*, vol.5, no.11(A), pp.3849-3860, 2009.
[6] S. Kobashi and Y. Hata, Lung lobar segmentation using tubular tissue density from multidetector-row CT images, *International Journal of Innovative Computing, Information and Control*, vol.6, no.3(A), pp.829-842, 2010.
[7] Z. Shi, L. Li, H. Wang, F. Wang, M. Zhao, Y. Wang and Q. Yao, Lung segmentation in chest radiographs using double localizing region-based active contours, *ICIC Express Letters, Part B: Applications*, vol.2, no.1, pp.69-74, 2011.
[8] Y. Zhang, Y. Mi and D. Huang, Fuzzy clustering image segmentation based on PSO, *ICIC Express Letters*, vol.5, no.3, pp.621-626, 2011.
[9] D. Kainmller, T. Lange and H. Lamecker, Shape constrained automatic segmentation of the liver based on a heuristic intensity model, *Proc. of MICCAI Workshop on 3-D Segmentat. Clinic: A Grand Challenge*, pp.109-116, 2007.
[10] D. Seghers, P. Slagmolen, Y. Lambelin et al., Landmark based liver segmentation using local shape and local intensity models, *Proc. of MICCAI Workshop on 3-D Segmentat. Clinic: A Grand Challenge*, pp.135-142, 2007.
[11] D. Furukawa, A. Shimizu and H. Kobatake, Automatic liver segmentation based on maximum a posterior probability estimation and level set method, *Proc. of MICCAI Workshop on 3-D Segmentat. Clinic: A Grand Challenge*, pp.117-124, 2007.
[12] E. Rikxoort, Y. Arzhaeva and B. Ginneken, Automatic segmentation of the liver in computed tomography scans with voxel classification and atlas matching, *Proc. of MICCAI Workshop on 3-D Segmentat. Clinic: A Grand Challenge*, pp.101-108, 2007.
[13] T. Heimann, H. Meinzer and I. Wolf, A statistical deformable model for the segmentation of liver CT volumes, *Proc. of MICCAI Workshop on 3-D Segmentat. Clinic: A Grand Challenge*, pp.161-166, 2007.
[14] M. Saddi, K. A. Rousson, C. Chefd'hotel et al., Global-to-local shape matching for liver segmentation in CT imaging, *Proc. of MICCAI Workshop on 3-D Segmentat. Clinic: A Grand Challenge*, pp.207-214, 2007.
[15] G. Schmidt, M. A. Athelogou, R. Schnmeyer et al., Cognition network technology for a fully automated 3-D segmentation of liver, *Proc. of MICCAI Workshop on 3-D Segmentat. Clinic: A Grand Challenge*, pp.125-133, 2007.
[16] Y. Chi, P. M. M. Cashman, F. Bello et al., A discussion on the evaluation of a new automatic liver volume segmentation method for specified CT image datasets, *Proc. of MICCAI Workshop on 3-D Segmentat. Clinic: A Grand Challenge*, 2007.
[17] F. Liu, B. S. Zhao, P. K. Kijewski et al., Liver segmentation for CT images using GVF snake, *Medical Physics*, vol.32, no.12, pp.3699-3706, 2005.
[18] L. Massoptier and S. Casciaro, A new fully automatic and robust algorithm for fast segmentation of liver tissue and tumors from CT scans, *European Radiology*, vol.18, no.8, pp.1658-1665, 2008.
[19] S.-J. Lim, Y.-Y. Jeong and Y.-S. Ho, Segmentation of the liver using the deformable contour method on CT images, in *Advances in Multimedia Information Processing – PCM 2005, Lecture Notes in Computer Science*, Y.-S. Ho and H. Kim (eds.), Springer Berlin/Heidelberg, 2005.
[20] L. Ruskó, G. Bekes et al., Fully automatic liver segmentation for contrast-enhanced CT images, *Proc. of MICCAI Workshop on 3-D Segmentat. Clinic: A Grand Challenge*, pp.143-150, 2007.
[21] P. Campadelli, E. Casiraghi and A. Esposito, Liver segmentation from computed tomography scans: A survey and a new algorithm, *Artif. Intell. Med.*, vol.45, no.2-3, pp.185-196, 2009.
[22] T. Heimann, B. van Ginneken, M. A. Styner et al., Comparison and evaluation of methods for liver segmentation from CT Datasets, *IEEE Transactions on Medical Imaging*, vol.28, no.8, pp.1251-1265, 2009.
[23] S. Maeda, H. Kim, Y. Itai, J. K. Tan, S. Ishikawa and A. Yamamoto, Reduction of processing times for temporal subtraction on lung CT image employing octree algorithms, *International Journal of Innovative Computing, Information and Control*, vol.7, no.5(B), pp.2603-2610, 2011.
[24] A. Krishnamurthy, J. Nehrbass, J. C. Chaves et al., Survey of parallel MATLAB techniques and applications to signal and image processing, *IEEE International Conference on Acoustics, Speech and Signal Processing*, 2007.
[25] O. Center and O. Columbus, Computational science IDE for HPCMP systems, *Users Group Conference*, 2007.

[26] R. Choy and A. Edelman, Parallel MATLAB: Doing it right, *Proc. of the IEEE*, vol.93, no.2, pp.331-341, 2005.
[27] N. T. Bliss and J. Kepner, pMATLAB parallel MATLAB library, *International Journal of High Performance Computing Applications*, vol.21, no.3, pp.336-359, 2007.
[28] R. Choy, A. Edelman, J. R. Gilbert et al., Star-P: High productivity parallel computing, *The 8th Annual Workshop on High-Performance Embedded Computing*, 2004.
[29] I. Mirman, Going parallel the new way, *Desktop Engineering*, vol.11, no.10, pp.24-25, 2006.
[30] J. Krupa, A. Pavelka, O. Vysata et al., Distributed signal processing, *Proc. of the Conference Technical Computing Prague*, Humusoft, Praha, 2007.
[31] P. Luszczek, Parallel programming in MATLAB, *International Journal of High Performance Computing Applications*, vol.23, no.3, pp.277-283, 2009.
[32] H. Pohlheim, S. Pawletta and A. Westphal, Parallel evolutionary optimization under Matlab on standard computing networks, *GECCO'99 – Proc. of the Genetic and Evolutionary Computation Conference – Workshop Program*, San Francisco, CA, USA, pp.174-176, 1999.
[33] D. Smith, *The MathWorks Introduces New Versions of MATLAB Parallel Computing Products*, The Mathworks Inc., http://www.mathworks.com/company/pressroom/articles/article34060.html., 2009.
[34] T. Kanungo, D. M. Mount, N. S. Netanyahu et al., An efficient k-means clustering algorithm: Analysis and implementation, *IEEE Transactions on Pattern Analysis and Machine Intelligence*, vol.24, no.7, pp.881-892, 2002.
[35] T. N. Pappas, An adaptive clustering-algorithm for image segmentation, *IEEE Transactions on Signal Processing*, vol.40, no.4, pp.901-914, 1992.
[36] S. Lankton and A. Tannenbaum, Localizing region-based active contours, *IEEE Transactions on Image Processing*, vol.17, no.11, pp.2029-2039, 2008.
[37] T. E. Chan, B. Y. Sandberg and L. A. Vese, Active contours without edges for vector-valued images, *Journal of Visual Communication and Image Representation*, vol.11, no.2, pp.130-141, 2000.
[38] M. Goryawala, M. Guillen, R. Bhatt et al., A comparative study on the performance of the parallel and distributing computing operation in MatLab, *IEEE the 24th International Conference on Advanced Information Networking and Application*, Perth, Australia, 2010.
[39] A. Beck and V. Aurich, HepaTux – A semiautomatic liver segmentation system, *Proc. of MICCAI Workshop on 3-D Segmentat. Clinic: A Grand Challenge*, pp.225-233, 2007.
[40] R. Beichel, C. Bauer, A. Bornik et al., Liver segmentation in CT data: A segmentation refinement approach, *Proc. of MICCAI Workshop on 3-D Segmentat. Clinic: A Grand Challenge*, pp.235-245, 2007.
[41] B. M. Dawant, R. Li, B. Lennon et al., Semi-automatic segmentation of the liver and its evaluation on the MICCAI 2007 grand challenge data set, *Proc. of MICCAI Workshop on 3-D Segmentat. Clinic: A Grand Challenge*, pp.215-221, 2007.
[42] J. Lee, N. Kim, H. Lee et al., Efficient liver segmentation exploiting level-set speed images with 2.5D shape propagation, *Proc. of MICCAI Workshop on 3-D Segmentat. Clinic: A Grand Challenge*, pp.189-196, 2007.
[43] R. Susomboon, D. S. Raicu and J. Furst, A hybrid approach for liver segmentation, *Proc. of MICCAI Workshop on 3-D Segmentat. Clinic: A Grand Challenge*, pp.151-160, 2007.